INTECH
open science | open minds

OPEN ACCESS
ARTICLE

Nanomaterials and Nanotechnology

Controlled Synthesis of TiO_2 Hierarchical Nanofibre Structures via Electrospinning and Solvothermal Processes: Photocatalytic Activity for Degradation of Methylene Blue

Regular Paper

Fredrick O. Ochanda[1,2,*], Sitarama Rajukada[1] and Matthew R. Barnett[1]

1 Centre for Materials and Fibre Innovation, Institute for Technology Research and Innovation Deakin University, Geelong, Australia
2 Currently at Department of Fibre Science and Apparel Design, Cornell University, NY, USA
* Corresponding author: frederick.ochanda@gmail.com

Received 25 May 2012; Accepted 18 July 2012

Abstract The present article describes a new titanium oxide-based (TiO_2) photocatalyst that shows promise for acceleration of dye degradation. A hierarchical TiO_2 nanostructure comprising nanorods on-nanofibres has been prepared using a sol–gel route and electrospinning. Calcination of electrospun nanofibre mats was performed in air at 500 °C. The TiO_2 nanofibre surface was then exploited as a 'seeding ground' to grow TiO_2 nanorods by a solvothermal process in NaOH. The nanofibres had a diameter of approximately 100 nm while the nanorods were evenly distributed on the nanofibre surface with a mean diameter of around 50–80 nm. The hierarchical nanostructure showed enhanced photocatalytic activity when compared to pure TiO_2 nanofibres. This improved efficiency in degrading methylene blue through the photocatalytic process was attributed to the larger specific surface area of the TiO_2 nanostructures, as well as high surface-to-volume ratio and higher reactive surface resulting in enhanced surface adsorption and interfacial redox reaction.

Keywords titanium oxide; hierarchical nanostructures; photocatalysts; electrospinning

1. Introduction

Many developing and developed nations are faced with a tremendous set of environmental problems related to the remediation of hazardous wastes, contaminated groundwaters and the control of toxic air contaminants. Groundwater contamination is one of the primary sources of human contact with toxic chemicals emanating from the textile and dyestuff manufacturing industry. Estimates indicate that approximately 15–20% of the synthetic textile dyes used are lost in wastewater streams

during manufacturing or processing operations.[1] Water contamination by methylene blue and similar dyes is a major environmental concern.[2,3] Some azo dyes and their degradation products, such as aromatic amines, are highly carcinogenic.[4] Proper treatment of the dye plant effluent is thus a matter of concern before discharge. This requires an innovation of the best technology, which can be efficiently used for the removal and remediation of dyes. Different approaches have been used for remediation of water contamination by dyestuffs. These approaches include: use of super absorbent polymer (SAP), filtration, flocculation, chemical precipitation, ion exchange, membrane separation, adsorption on a high surface area activated carbon[5-6] and photocatalytic oxidation by semiconductors.

Photocatalytic oxidation of dyes using titanium oxide is the most promising technology among the different methods. A significant contribution to this technology is attributed to the pioneering work of Matthews et al.[7] who have researched extensively photocatalytic destruction of organic contaminants in water. Due to the potentiality of photocatalysis, there has been continued intensive research undertaken in recent years to enhance its effectiveness.[8-12] Despite this research enhancing the efficiency to meet practical application requirements is still a challenge. Part of the problem is the poor quantum yield caused by the rapid recombination of photogenerated electrons and holes.[13] In addition, TiO_2 has primarily been used in particulate form, which suffers loss of particles during photocatalytic application.[14] Various methods have been formulated to resolve these problems, such as foreign element doping, [15] immobilization of TiO_2 on substrates[16-17] and development of advanced materials with hierarchical nanostructures.[18]

Synthesis of hierarchical nanostructures with controllable sizes, shapes and compositions has received increased attention in recent years.[19] These complex architectures, especially those based on one-dimensional nanostructures, are expected to display novel functions important to the development of advanced devices and systems. Recent examples include hierarchically structured nanowires (e.g., nanowire-on-nanowire, nanorod on-nanofibre) of ZnO/In_2O_3, SnO, ZnO, SnO_2-doped In_2O_3, GaP/Ga(As)-P, SnO_2/Fe_2O_3, SnO_2/TiO_2 and TiO_2/V_2O_5 hierarchical.[19] Such advances in complex architectures may hold the key to highly efficient photocatalysts useful in the degradation of environmental contaminants. An advantage of using TiO_2 nanofibres and/or hierarchical nanostructures as opposed to particulate films is that they enable more efficient charge separation due to the absence of grain boundaries typical in particulate films.[20]

The present study examines the potential to employ hierarchical TiO_2 nanostructures, with a large aspect ratio, as photocatalysts for the degradation of methylene blue. We demonstrate for the first time successful growth of TiO_2 nanorods on the surface of TiO_2 nanofibres by combining sol-gel, electrospinning and solvothermal methods. For the first time, we show that these hierarchical nanostructures exhibit superior photocatalytic efficiency over pure TiO_2 nanofibres in the decolouration of methylene blue.

2. Experimental Procedures

2.1 Electrospinning of TiO_2 nanofibres

Raw materials for fabrication included analytical reagent (AR) grade NaOH pellets, dimethyl-n'n-formamide (DMF), chloroform ($CHCl_3$), ammonium hydroxide solution, polyvinyl pyrollydone (PVP) and titanium isopropoxide (Ti (Iso)), all from Sigma Aldrich Pty. Ltd. Sydney, Australia. Briefly, a sol–gel composed of Ti (Iso) and PVP was prepared as follows: 1.2 g of PVP was dissolved in DMF/$CHCl_3$ solvent mixture in a 2:1 ratio to make a 13 wt% solution, followed by addition of 0.5 g of Ti (Iso). The resulting mixture was stirred and then few drops (3-5) of ammonia solution were added to induce hydrolysis and condensation of the sol. A high voltage power supply (D-ES50PN-5W/DDPM, Gamma High Voltage Research Inc, Ormond Beach, FL) was used as a source of electric field with an applied voltage of 20 kV and nozzle to collector distance of 20 cm. The sol–gel was supplied through a plastic syringe attached to a capillary tip with a solution pump rate of 0.30 ml/h. A copper wire originating from the positive electrode (anode) was attached to the needle and a negative electrode (cathode) was attached to a metallic collector covered with aluminium foil. The resulting fibres were heat treated to 500 ^oC in air at 10 ^oC/min and held at that temperature for 3 h before allowing to cool at 10 ^oC/min using a Thermo Fisher Scientific Lindberg/Blue M Mini-Mite Tube Furnace (Scoresby, Victoria, Australia).

2.2 Solvothermal synthesis of TiO_2 nanorods on nanofibre surface

TiO_2 hierarchical structures were fabricated through a solvothermal reaction between NaOH solution and the mixture of TiO_2. In a typical synthesis, 0.5 g of TiO_2 nanofibres was added to 15 mL of 4 M NaOH aqueous solution. A 15 mL ethanol solvent was added to this solution followed by heating in a 50 mL Teflon lined autoclave at 150 °C for 12 h. Three additional samples were prepared following the same procedure allowing the reaction to proceed for 0.5, 1.0 and 6.0h in the autoclave. The precipitate was washed with distilled water and absolute ethanol in that order, and then dried in air.

2.3 Morphology and microstructure analysis

Morphology and microstructure analysis was carried out using scanning (SUPRA-55VP-FEGSEM) and transmission electron microscopy (JEOL JEM 2100). X-ray powder diffraction (XRD) patterns were obtained with a Philips diffractometer using monochromatized Cu Kα radiation. The absorption edge of the TiO_2 was determined using a Varian UV-Vis spectrophotometer equipped with an integrating sphere. The BET surface area of the hierarchical TiO_2 nanostructures and TiO_2 nanofibre was obtained with nitrogen adsorption in a Micrometrics TriStar 3000 Surface Area and Porosity Analyser (Particle & Surface Sciences Pty. Limited, Gosford, New South Wales Australia). BET surface area was calculated from the BET plot. Pore-size distributions were calculated using the BJH model. The pore volume was measured at the single point of $p/p_0 = 0.99$. Helium gas was used for dead space measurements and nitrogen was employed as an adsorbate gas.

2.4 Photocatalytic study

Methylene blue (MB) was used to evaluate the photocatalytic activity of titanium oxide and the hierarchical nanostructure materials in response to UV and visible irradiation. The optical absorption peak of MB at 660 nm was chosen to monitor the photocatalytic degradation process. According to the Lambert-Beer law, [21] the concentration of methylene blue solutions can be obtained from this characteristic absorption peak. The experiment was conducted according to the following procedure: 50 mg/L methylene blue solution was prepared to a 150 mL volume in a 200 mL beaker. To this solution, a 50 mg of dried nanofibre catalyst was dispersed to make a suspension. The concentration of the catalyst was set constant for all the experiments. The suspension was stirred in the dark for 1h to ensure the establishment of adsorption and desorption equilibrium of MB on the nanofibre surface. Subsequently the suspension was irradiated with simulated sunlight using an Atlas Suntest CPS+ instrument (Atlas Co., Chicago, IL) equipped with a 150W xenon lamp and a filter (coated quartz dish). The suspension was gently stirred throughout the course of the experiment to maintain its stability. At given intervals, 5 mL of the suspension was extracted and then centrifuged at 6000 rpm for 15 min to separate the nanofibres from the supernatant. A Varian Cary 3E spectrophotometer (Varian Co., Mulgrave, Australia) was used to generate time-dependent absorbance changes of the supernatant at the wavelength between 400 and 800 nm.

3. Results and Discussion

3.1 SEM and TEM micrographs analyses

The overall morphology and a high-magnification SEM micrograph of the electrospun TiO_2 nanofibres can be seen in Figure 1A. The onset of the solvothermal reaction is shown in Figure 1B. It is observed from the SEM micrographs that the solvothermal titanium oxide product after further reaction time contains numerous flower-like aggregates (Figure 1C). These flower-like aggregates (Figure 1D, 1E) consist of high density nanorods with a diameter of 50-70 nm. The length of these nanorods can be modulated by controlling the reaction time. With the reaction time shorter than 0.5 h, only bare TiO_2 nanofibres were observed. With the reaction prolonged to 1.0 h, a layer of nanoparticles with a thickness of a few nanometres deposited on the surface of the TiO_2 nanofibres could be observed. When the

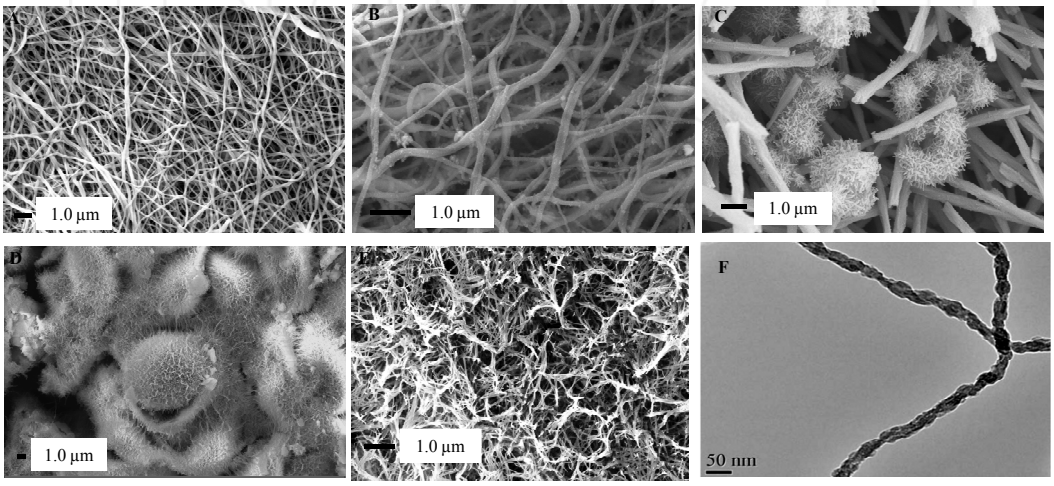

Figure 1. SEM micrographs of TiO_2: (a) pure electrospun TiO_2, (b) 1 h solvothermal treatment showing TiO_2 particle nucleation on nanofibre surface. (C) Hierarchical TiO_2 after solvothermal treatment for 6 h showing the onset of nano-scale flower-like coverage of nanofibre surface, (D) for 12 h showing nano-scale flower-like nanostructures completely covering the nanofibre surface. (E) Expanded view of (D) showing the nanorod network, (F) TEM micrograph shows the microstructure of the nanorods.

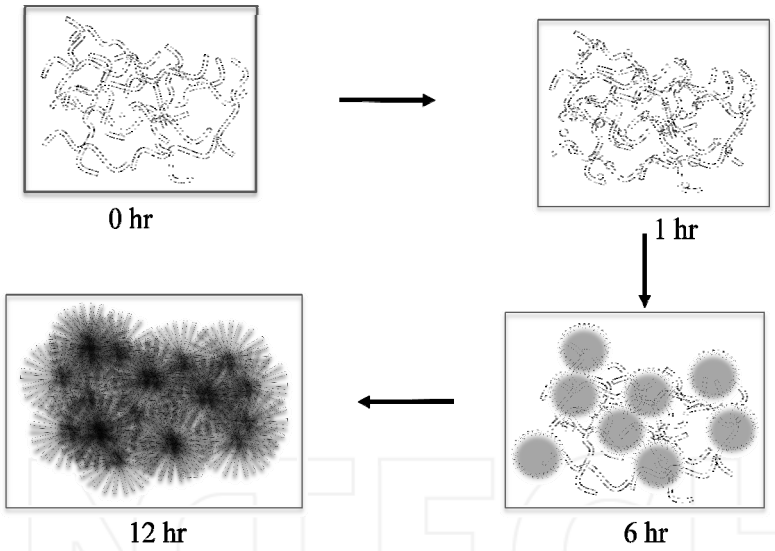

Scheme 1. Schematic illustration of the growth process of the hierarchical TiO_2 nanostructures from solvothermal reaction.

reaction was allowed to proceed for 6 h, the nano-scale flower-like nanostructures nucleated from the particles on the nanofibre surface, but did not cover the surface completely. Extending the reaction to 12 h caused nano-scale flower-like nanostructures to grow into arrays of nanorods with a length of around 50-70 nm. The TEM micrograph (Fig. 1F) shows a nodular type of microstructure, indicating that the nanorods' growth started from homogenous nucleation of TiO_2 nanoparticles. This is consistent with the SEM micrograph in Figure 1B. The growth process of the hierarchical TiO_2 nanostructures from solvothermal method is illustrated schematically by Scheme 1.

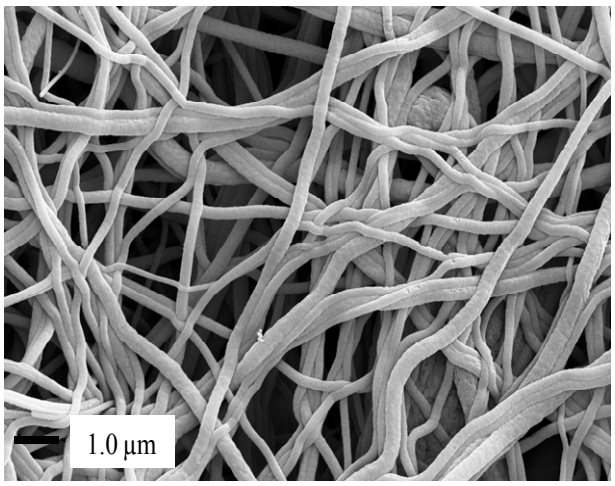

Figure 2. SEM micrograph of TiO_2 nanofibres after 12 h solvothermal treatment (no NaOH) showing formation of pores or dimples on fibre surfaces.

When TiO_2 is reacted with NaOH solution, some of the Ti–O–H (and Ti–O–Ti) bonds are broken and this results in the formation of a layered structure of titanate.[22] It is observed that the aspect ratio and length of the nanorods which gradually grow from the surface of TiO_2 particles are affected by the reaction time. During the process of solvothermal treatment, 1D TiO_2 polycrystals are formed on the nanofibre surface by anisotropic growth. The results show that, in the ethanol solvent medium, TiO_2 nanofibres can provide a source for the nucleation of particles, followed by the anisotropic growth of TiO_2 rods on the particle surface. This results in a hierarchical structure. It was also observed that the addition of NaOH aqueous solution for pH adjustment was important for the nanorod growth, as experiments with no NaOH did not yield hierarchical nanostructures as shown in Figure 2.

	BET (m⁻²g)	Pore Diameter (⁻)	Pore Volume (cm⁻³g)
TiO_2 Nanofibres	52.43	44.67	0.0684
TiO_2 Hierarchical Nanostructures	94.01	58.94	0.1043

Table 1. Comparing surface area of hierarchical TiO_2 nanostructures and pure TiO_2 nanofibres.

N_2 adsorption–desorption isotherms of the synthesized TiO_2 nanofibres and hierarchical nanostructures were measured using Micrometrics TriStar 3000 Surface Area and Porosity Analyser after the samples were degassed in a vacuum at 250 °C for 3 h. As can be seen from Table 1, the hierarchical TiO_2 nanostructure sample exhibits better nitrogen adsorption than pure TiO_2 nanofibres which is reflected in the BET surface area. Table 1 summarizes the surface area data, with BET surface area, pore volume and pore diameter of hierarchical TiO_2 nanostructures much higher than those of pure TiO_2 nanofibres. The surface area results are consistent with the higher degradation efficiency of methylene blue over hierarchical TiO_2 nanostructures discussed in section 3.3.

3.2 Optical spectroscopy and XRD studies of hierarchical titanium oxide nanofibres

Measurement of diffuse reflectance with a UV-visible spectrophotometer is a standard technique in the determination of the absorption properties of materials. This information can be used to estimate the band-gap energy (also referred to as the band gap) of semiconductor materials. Determination of the band gap from the measurement of the diffuse reflectance of a powder or fibrous sample is a standard technique.[23-24] UV-visible diffuse reflectance spectra of the hierarchical TiO_2 nanostructures calcined at 500 °C is shown in Figure 3. Over the range of 350–400 nm an abrupt increase in the reflectance is observed which indicates the onset of the fundamental absorption edge. This is typical of titanium oxide and provides a clear indication of successful synthesis of the same. Based on reflectance spectra, the absorption edge was determined to occur at a frequency of ~ 385 nm. Using this absorption edge value, the band gap energy was estimated to be ~ 3.22 eV from the relationship of photon energy and frequency $E=h\nu$, where h is Planck's constant (6.626×10^{-34} J s) and $\nu = c/\lambda$; where c is the speed of light (2.998×10^{8} ms^{-1}) and λ is the wavelength of light.

The structure of the hierarchical TiO_2 nanostructure was studied using the powder x-ray diffraction method. The samples were ground into fine powders and mounted on zero-background diffraction holders. The XRD analysis was completed from 10-70 degrees two-theta with a 0.02 degree step and a 1 second dwell. The XRD pattern of hierarchical TiO_2 is shown in Figure 4. The structure can be indexed to TiO_2 in the anatase-rutile mixed phase with the interplanar d-spacings indexed to 101, 103, 105, 200, 202, 204, 210, 211, 213, 220, 320 and 004 reflections. The broad diffraction peaks are due to crystallite size broadening resulting from the nanocrystalline particle size. The crystallite size 'D' was determined from the 103 peak in the XRD pattern (chosen for its high intensity) using the Debye–Scherrer formula [25]

$$D = \frac{0.94\lambda}{\beta \cos\theta},$$

where λ is the wavelength of CuK_α radiations (1.54 Å), β the full-width at half-maximum of the peak corresponding to the plane {1 0 3} and θ the angle obtained from 2θ value corresponding to the maximum intensity peak in the XRD pattern. The diameter of crystallite size of obtained TiO_2 particles was ~ 4 nm.

The background of the x-ray pattern (Figure 4) is flat, indicating that electrospun TiO_2 is crystalline. It is obvious that the nanostructures are polycrystalline titanium oxide (TiO_2) with a predominantly anatase crystal structure.

3.3 Photocatalytic evaluation

The UV–Vis spectral change of 50 mg L^{-1} methylene blue as a function of irradiation time during the course of photodegradation by the TiO_2 and hierarchical TiO_2 nanofibre photocatalysts are shown in Fig. 5 and Fig. 6, respectively. The intensity was normalized with the initial value at the beginning of irradiation. With time increasing from 0 to 150 min, the intensity of the characteristic absorption band at peaks of 660 nm decreased gradually, suggesting that the methylene blue was gradually photodegradated by the TiO_2 and hierarchical TiO_2 nanofibre photocatalysts. After 120-150 minutes the methylene blue was almost completely removed from the solution.

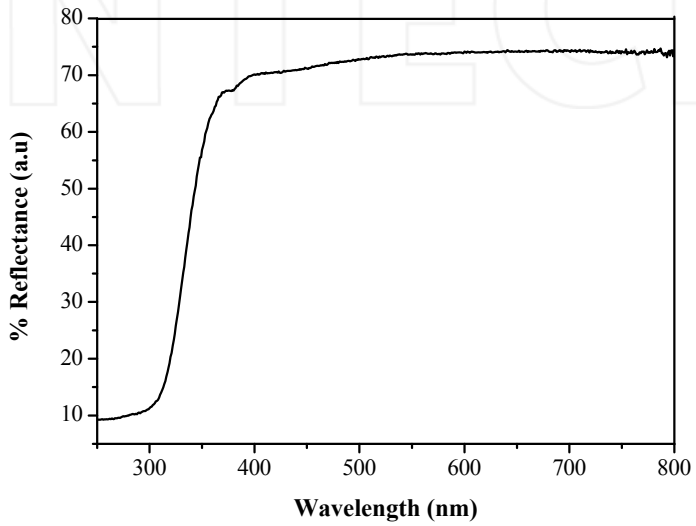

Figure 3. UV-visible diffuse reflectance spectra of the hierarchical TiO_2 nanostructures.

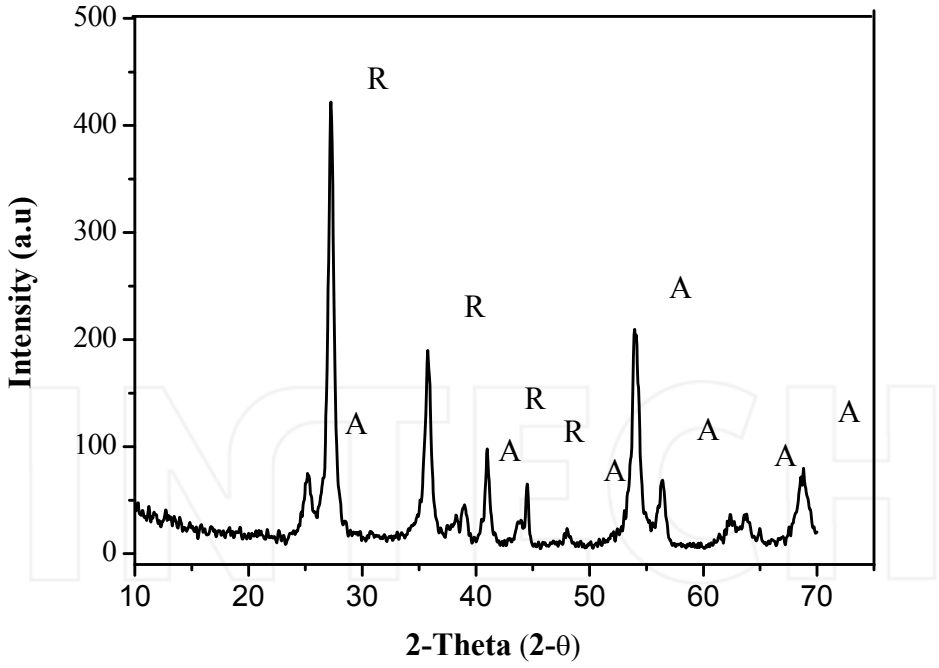

Figure 4. XRD spectra of hierarchical titanium oxide nanofibres showing the mixed phase after solvothermal treatment. (A=Anatase, R=Rutile).

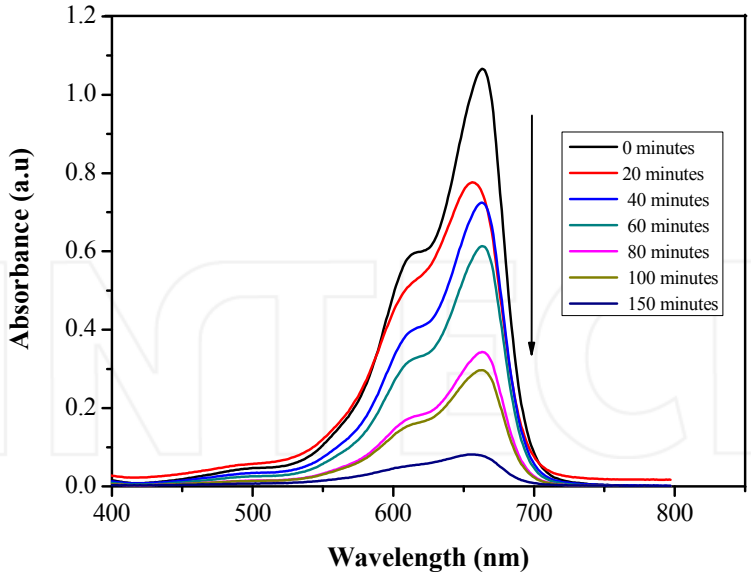

Figure 5. UV–Vis absorption spectra of photocatalytic degradation methylene blue recorded at different time intervals by the TiO_2 nanofibre catalyst.

When TiO_2 is illuminated by UV light, electrons are excited from the valence band to the conduction band generating electron-hole pairs.[26] The holes in TiO_2 will react with water molecules or hydroxide ions and produce hydroxyl radicals. Oxygen is usually supplied as an electron acceptor to prolong the recombination of electron-hole pairs during photocatalytic oxidation. The hydroxyl radical is a powerful oxidizing agent and attacks organic pollutants present at or near the surface of TiO_2.[27] This causes photo-oxidation of pollutants according to the following processes: (i) photo-absorption of the semiconductor catalyst; (ii) the generation of electrons and holes; (iii) the transfer of charge carriers, and (iv) the utilization of the charge carriers by the reactants.

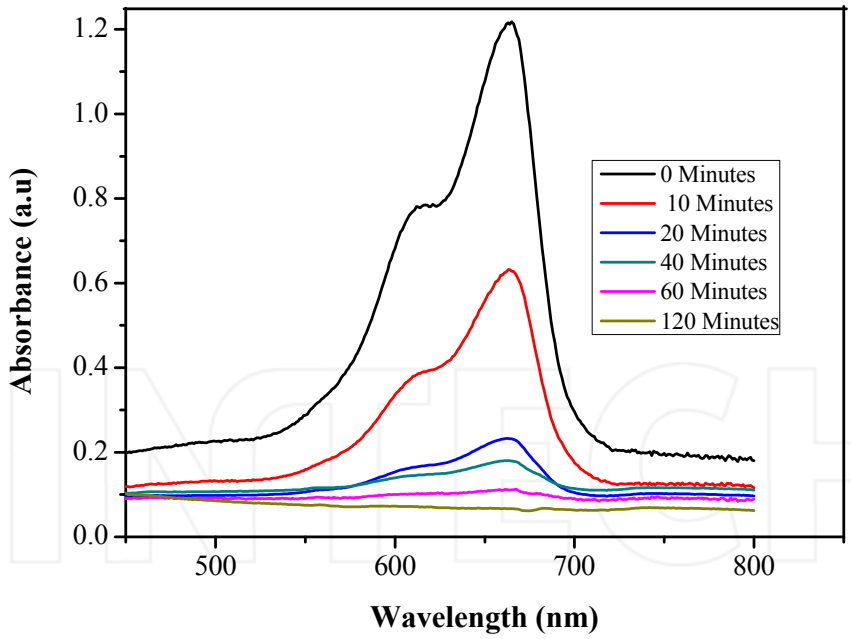

Figure 6. UV–Vis absorption spectra of photocatalytic degradation methylene blue recorded at different time intervals by the hierarchical TiO_2 nanostructures catalyst.

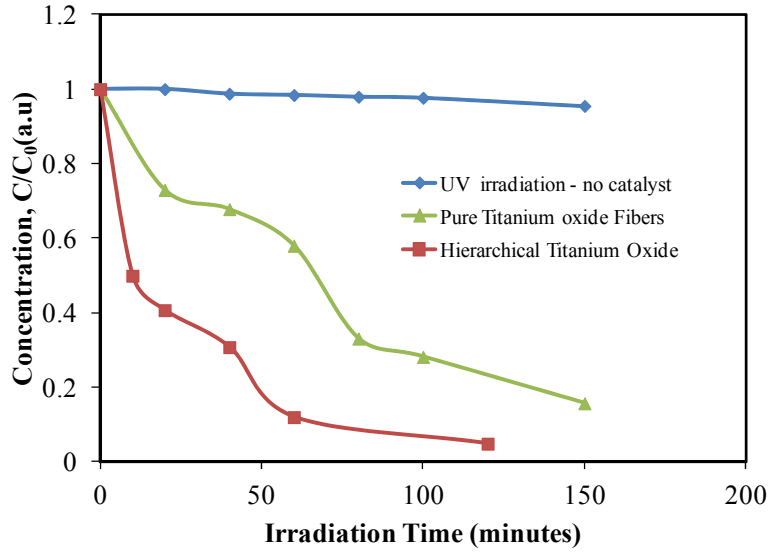

Figure 7. Time-dependent photodegradation of methylene blue under different conditions. The weight of catalyst used was kept constant in all cases.

Time-dependent photodegradation of methylene blue is illustrated in Figure 7. It is shown that methylene blue decomposes in the presence of nanofibre and nanostructured TiO_2 nanofibre under illumination by UV light. From Figure 7, it is observable that the photocatalytic ability of the hierarchical TiO_2 nanostructures is greater than that of the pure TiO_2 nanofibres. This suggests that hydrothermally modified TiO_2 possesses improved the efficiency of the electron-transfer dynamics.

4. Mechanism and Rate Equation

According to much of the literature, when an aqueous solution is irradiated in the presence of TiO_2 catalyst, the adsorbed water molecules react with holes in the valence band to form hydroxyl radicals and release of hydrogen ions. In addition, the dye molecules might be decomposed to form organic acids as the intermediate products. In our experiments, methylene blue solutions were pre-mixed with the TiO_2 suspension before the UV

light was turned on to excite the TiO_2 nanostructures. Therefore, it was anticipated that the adsorption of methylene blue onto the TiO_2 nanostructure surface should be the first step in the reaction mechanism. Methylene blue-adsorbed TiO_2 nanostructures were then excited to generate hydroxyl and superoxide radicals which both participate in decomposition of the adsorbed methylene blue. The reaction steps for the decomposition of methylene blue can be summarized as:[28-30]

$$TiO_2 + dye \leftrightarrow TiO_2 - dye \quad (1)$$

$$TiO_2 - dye + h\upsilon \leftrightarrow TiO_2(e^-, h^+) - dye \quad (2)$$

$$TiO_2(h^+) + H_2O_{(ads)} \rightarrow TiO_2(OH_{(ads)}\bullet) + H^+ \quad (3)$$

$$TiO_2(h^+) + OH^-_{ads} \rightarrow TiO_2(OH_{(ads)}\bullet) \quad (4)$$

$$TiO_2(e^-) + O_{2(ads)} \rightarrow TiO_2(O^-_{2(ads)}\bullet) \quad (5)$$

$$OH_{(ads)}\bullet + dye \rightarrow intermediate\ products \rightarrow degradation\ products \quad (6)$$

$$O^-_{2(ads)}\bullet + dye \rightarrow intermediate\ products \rightarrow degradation\ products \quad (7)$$

The photodegradation efficiency for each experiment, also called conversion, is calculated by the following relation:

$$X(\%) = \frac{C_0 - C}{C_0} x100 \quad (8)$$

where X is the photodegradation efficiency, C_o the concentration of methylene blue before illumination and C the concentration of methylene blue in suspension after time t (mg L^{-1}).

It is expected that more dye molecules are adsorbed on the surface of the hierarchical TiO_2 nanostructures than on the TiO_2 nanofibre surface. This would increase the photoexcited electron transfer from the sensitized dye molecule to the conduction band of TiO_2 and consequently increase the electron transfer to any adsorbed O_2. It is likely that the TiO_2 nanorods generated on the surface of TiO_2 nanofibres enhance the reaction between photo-generated charges and O_{2^-} or OH^- species on the surface better than pure TiO_2 nanofibres. The higher photocatalytic activity over the hierarchical nanostructures can be attributed to the efficient capture of reflected and refracted light by the radially outward oriented TiO_2 nanorods formed over the circumference of the titanium nanofibres. The formation of TiO_2 nanorods over TiO_2 nanofibres can be considered as an effective alternate to improve photodegradation rates by avoiding expensive additives.[31] In addition, the nanorods in the hierarchical structure have high aspect ratio and nanoscale diameter which can promote accumulation of photoexcited electrons on the top ends of TiO_2 nanorods thereby retarding electron-hole recombination.[32] In nanostructured TiO_2, the surface-to-volume ratio is very high and hence the reactive surface is also higher in this regime. Therefore, the surface adsorption and interfacial redox reaction is enhanced by using nanostructured materials.

The reaction rate for photocatalytic reactions is independent of hydroxyl concentration[33], therefore, a pseudo first-order kinetic model was used to fit the experimental data:

$$\frac{-dC_{MB}}{dt} = kC_{MB}C_{OH^*} \quad (9)$$

where C_{MB} represents the dye concentration, mg/L; C_{OH^*} represents the hydroxyl radical concentration, mg/L;

By the pseudo-stationary hypothesis (i.e., the C_{OH^*} can be considered to be a constant in the presence of excess O_2), the rate expression (1) can be simplified to fit an equation following the first-order kinetics,

$$\frac{-dC_{MB}}{dt} = kC_{MB} \quad (10)$$

Integrating the above equation; from 'C_{MB0}' to 'C_{MB}'on the left hand side, and '0' to't' on the right;

$$\int_{C_{MB0}}^{C_{MB}} -dC_{MB} = k\int_0^t dt$$
$$\ln(C_{MB0} / C_{MB}) = kt \quad (11)$$

where C_{MB0} represents the initial dye concentration in mg/L, k is pseudo first-order rate constant (min^{-1}), t is time interval (min) and C_{MB} represents the final dye concentration in mg/L.

The degradation rate data obtained for hierarchical TiO_2 and TiO_2 nanofibre concentration were plotted using the pseudo first-order kinetic model. The fairness of the fit is indicated by the fact that the linear regression (R^2) values were 0.84 and 0.95 for hierarchical TiO_2 and TiO_2 nanofibres, respectively. Therefore, the model is in good agreement with the experimental data. The values of the first-order rate constant (k) and degradation efficiency (X) are indicated in Table 2 below. The value of k is 0.052 and 0.0132 min^{-1} and efficiency (120 and 150minutes) are 94.6 and 92.5% for hierarchical TiO_2 nanostructures and pure TiO_2 nanofibres, respectively. From the results it can be interpreted that the rate of degradation of methylene blue dye is faster for

hierarchical titanium oxide than pure titanium oxide for dye concentration of 50 mg/L. The change in degradation efficiency with time for these samples is represented in Figure 8. We ascribe the enhanced kinetics of photocatalytic degradation of methylene blue to the higher surface area and peculiar morphology of solvothermally grown samples. In fact, for given conditions, the reaction rate is directly proportional to the fraction of catalytically active surface covered by methylene blue.

Catalyst	Rate (min^{-1})	Efficiency (%)
Hierarchical Titanium oxide	0.052±0.02	94.6 (120 min)
Pure Titanium Oxide	0.0132±0.013	92.5 (150 min)

Table 2. Comparison of rate constants and degradation efficiency for the degradation of methylene blue by hierarchical TiO_2 nanostructures and pure TiO_2 nanofibres.

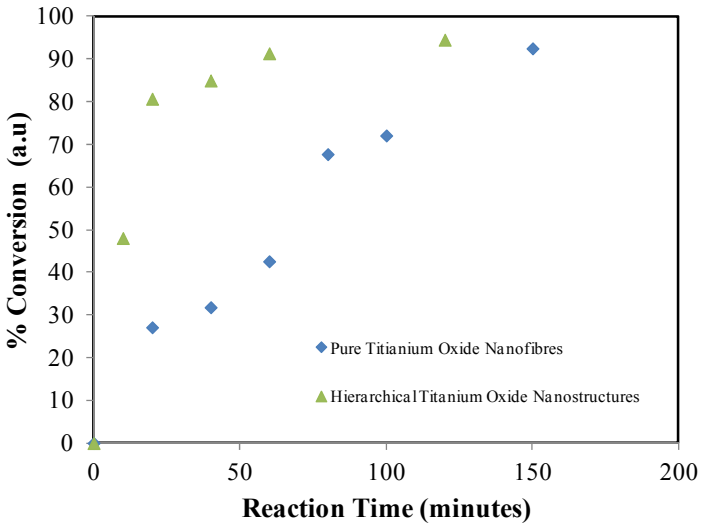

Figure 8. Degradation efficiency (% conversion) of Pure TiO_2 nanofibres and hierarchical TiO_2 nanostructures.

5. Conclusion

In this work, hierarchical TiO_2 nanaostructures were prepared by first fabricating TiO_2 through a sol–gel route and electrospinning process followed by a solvothermal process in NaOH. A hierarchical (nanorod on nanofibre) structure was formed using an NaOH solvothermal process. We have also observed that no nanorods were formed when no NaOH was added to titanium oxide during the solvothermal process. Compared with titania nanofibres, the hierarchical titania nanostructures showed an increased photocatalytic activity. This improved efficiency in degrading methylene blue through the photocatalytic process is attributed to the larger specific surface area of the TiO_2 nanostructures, as well as high aspect ratio. The surface-to-volume ratio is very high, and hence, the reactive surface is also higher resulting in enhanced surface adsorption and interfacial redox reaction. This kind of TiO_2 hierarchical structured material promises high potential and significant large-scale applications in environmental photocatalysis.

6. Acknowledgements

This work was supported by Alfred Deakin Postdoctoral Fellowship and Division of Research Services, Deakin University.

7. References

[1] *Pollution Prevention and Abatement Handbook, World Bank Group, Washington, DC,* 1998, ISBN: 0-8213-3628-X.
[2] Walker, G.M.; Hansen, L.; Hanna, J.A.; Allen, S.J. *Water Res.* 2003, 37, 2081.
[3] Stydini, M.; Dimitris, I.K.; Verykios, X.E. *Appl. Catal. Environ.* 2004, 47, 189.
[4] Mohamed, M.M. *J. Colloid and Interface Science* 2004, 272, 28.
[5] Mondal, S. *Env. Eng. Sci.* 2008, 25, 383.
[6] Rai, H.S.; Bhattacharyya, M.S.; Singh, J.; Bansal, T.K.; Vats, P.; Banerjee, U.C. *Crit. Rev. Env. Sci. Technol.* 2005, 35, 219.
[7] Mathews, R.W; McEvoy, R.S *Solar Energy* 1992, 49, 507-513.
[8] Matthews, R.W. *War. Res.* 1991, 25, 1169-1176.
[9] Matthews, R.W.; Abdullah, M.; Low, G.K.-C. *Anal. Chem. Acta* 1990, 233, 171-179.
[10] Matthews, R.W. *J. Catal.* 1988, 111, 549-555.
[11] Matthews, R.W. *Wat. Res.* 1986, 20, 569-578.
[12] Hoffmann, M.R.; Martin, S.T.; Choi, W.Y.; Bahnemann, D.W. *Chem. Rev.* 1995, 95, 69.
[13] Arslan, I.; Balcioglu, I.A.; Bahnemann, D.W. *Appl. Catal. B: Environ.* 2000, 26, 193.
[14] Pelizzetti, E.; Minero, C. *Electrochim. Acta* 1993, 38, 47.

[15] Bhatkhande, D.S.; Pangarkar, V.G.; Beenackers, A.A.C.M. *J. Chem. Technol. Biot.* 2002, 77, 102.
[16] Schmelling, D.C.; Gray, K.A.; Kamat, P.V. *Water. Res.* 1997, 31, 1439.
[17] Zhang, X.; Zhang, Y.; Quan, X.; Chen, S. *Journal of Hazardous Materials* 2009, 167, 911.
[18] Zhang, X.; Zhou, M.; Lei, L. *Carbon* 2005, 43 (8), 1700.
[19] Lv, Y.Y.; Ding, Y.; Zhou, J.H.; Xiao, W.M.; Feng, Y.Y. *J. Am. Ceram. Soc*. 2009, 92 (4), 938.
[20] Kim, C.; Kim, J.T.; Kim, K.S.; Jeong, S.; Kim, H.Y.; Han Y.S. *Electrochimica Acta* 2009, 54(24), 5715.
[21] Guillard, C.; Disdier, J.; Monnet, C.; Dussaud, J.; Malato, S.; Blanco, J.; Maldonado, M.I.; Herrmann, J.M. *Appl. Catal. B: Environ.* 2003, 46, 319.
[22] Zhang, Z.; Shao, C.; Li, X.; Zhang, L.; Xue, H.; Wang, C.; Liu, Y. *J. Phys. Chem. C* 2010, *114,* 7920.
[23] Lauhon, L.J.; Gudiksen, M.S.; Wang, D.; Lieber, C.M. *Nature* 2002, 420, 57.
[24] Milliron, D.J.; Hughes, S.M.; Cui, Y.; Manna, L.; Li, J.; Wang, L.-W.; Alivisatos, A.P. *Nature* 2004, 430, 190.
[25] Jun, Y.-W.; Lee, S.-M.; Kang, N.-J.; Cheon, J. *J. Am. Chem. Soc.* 2001, 123, 5150.
[26] Lao, J.Y.; Wen, J.G.; Ren, Z.F. *Nano Lett.* 2002, 11, 1287.
[27] Wang, Z.L.; Pan, Z.W. *Ad*V. *Mater.* 2002, 14, 1029.
[28] Gao, P.; Wang, Z.L. *J. Phys. Chem. B* 2002, 106, 12653.
[29] Wan, Q.; Wei, M.; Zhi, D.; MacManus-Driscoll, J.L; Blamire, M.G. *Ad*V. *Mater.* 2006, 18, 234.
[30] Dick, K.A.; Deppert, K.; Larsson, M.W.; Martensson, T.; Seifert, W.; Wallenberg, L.R.; Samuelson, L. *Nat. Mater.* 2004, 3, 380.
[31] Zhang, D.-F.; Sun, L.-D.; Jia, C.-J.; Yan, Z.-G.; You, L.-P.; Yan, C.-H. *J. Am. Chem. Soc.* 2005, 127, 13492.
[32] Ostermann, R.; Li, D.; Yin, Y.; McCann, J.T., Xia, Y. *Nano Lett*. 2006, 6 (6), 1297.
[33] Liu, Z.; Zhang, X.; Nishimoto, S.; Jin, M.; Tryk, D.; Murakami, T.; Fujishima, A. *J. Phys. Chem. C* 2008, 112, 253.
[34] Ingle, J.D.J.; Crouch, S.R. *Spectrochemical Analysis*; Prentice Hall: Englewood Cliffs, NJ, 1988.
[35] Rhee, C.H.; Bae, S.W.; Lee, J.S. Chem. Lett. 2005, 34, 660.
[36] Karvaly, B.; Hevesi, I. Z. *Naturforsch*. 26a 1971, 245.
[37] Wendlandt, W.W.; Hecht, H.G. *Reflectance Spectroscopy*, Wiley Interscience, New York, 1966.
[38] West, A.R. *Solid State Chemistry and its Application*, Wiley, New York 1984, pp. 174.
[39] Yu, D.Z.; Cai, R.X.; Liu, Z.H. *Spectrochim. Acta A* 2004, 60 (7), 1617.
[40] Legrini, O.; Oliveros, E.; Braun, A.M. *Chem. Rev*. 1993, 93 (2), 671.
[41] Fujishima, A.; Rao, T.N.; Tryk, D.A. *J. Photochem. Photobiol. C* 2000, 1, 1.
[42] Habibi, M.H.; Hassanzadeh, A.; Mahdavi, S. *J. Photochem. Photobiol. A* 2005, 172, 89.
[43] Gaalindo, C.; Jacques, P.; Kalt, A. *J. Photochem. Photobiol. A* 2000, 130, 35.
[44] Archana, K.; York, R.S.; Vaidyanathan, S. *Environ. Sci. Technol.* 2009, *43,* 3260.
[45] Kang, S-Z.; Xu, Z.; Song, Y.; Mu, J. *J. Dispersion Sci. Technol.* 2006, 27, 857.
[46] Guettai, N; Amar, H.A. *Desalination* 2005, 185, 427-437.